Polarization engineering via staggered InGaN quantum wells for radiative efficiency enhancement of light emitting diodes

Ronald A. Arif, Yik-Khoon Ee, and Nelson Tansu

Citation: Appl. Phys. Lett. **91**, 091110 (2007); doi: 10.1063/1.2775334
View online: http://dx.doi.org/10.1063/1.2775334
View Table of Contents: http://apl.aip.org/resource/1/APPLAB/v91/i9
Published by the American Institute of Physics.

Polarization engineering via staggered InGaN quantum wells for radiative efficiency enhancement of light emitting diodes

Ronald A. Arif,[a] Yik-Khoon Ee, and Nelson Tansu[b]
Center for Optical Technologies, Department of Electrical and Computer Engineering, Lehigh University, 7 Asa Drive, Bethlehem, Pennsylvania 18015

(Received 17 May 2007; accepted 2 August 2007; published online 27 August 2007)

Staggered InGaN quantum wells (QWs) grown by metal-organic chemical vapor deposition are demonstrated as improved active region for visible light emitters. Theoretical studies indicate that InGaN QW with step-function-like In content in the quantum well offers significantly improved radiative recombination rate and optical gain in comparison to the conventional type-I InGaN QW. Experimental results of light emitting diode (LED) structure utilizing staggered InGaN QW show good agreement with theory. Polarization band engineering via staggered InGaN quantum well allows enhancement of radiative recombination rate, leading to the improvement of photoluminescence intensity and LED output power. © *2007 American Institute of Physics*.
[DOI: 10.1063/1.2775334]

Conventional III-nitride active media for lasers and light emitting diodes (LEDs) emitting in the visible regime is based on InGaN quantum wells (QWs).[1–7] Two major challenges that hinder high performance conventional InGaN QW LEDs and lasers are (1) the high defect density and phase separation in InGaN QW and (2) the existence of inherent electrostatic field. The high threading dislocation density in III nitrides leads to low radiative efficiency, while the intrinsic electrostatic fields result in significant reduction of electron-hole wave function overlap ($\Gamma_{e\text{-hh}}$).[8–11]

In conventional InGaN QW, the inherent spontaneous and piezoelectric polarization fields result in energy band bending, which in turn leads to spatial separation of electron and hole wave functions in the QW. Previously, the dependence of transition matrix element on In content in 30 Å InGaN QW had been shown.[12] To illustrate the charge separation effect, we have calculated emission wavelength and overlap $\Gamma_{e\text{-hh}}$ of 25 Å type-I InGaN QW. As the In content in the InGaN QW is increased, the overlap $\Gamma_{e\text{-hh}}$ reduces to 27.7% for emission wavelength at 531.9 nm.

In this work, we present an approach to improve radiative recombination rate and efficiency in nitride-based active media by utilizing staggered InGaN QW with step-function-like In content profile in the QW. According to Fermi's golden rule, the electronic transition from state $|2\rangle$ to $|1\rangle$ is governed by transition matrix element via the perturbation Hamiltonian $\hat{H}'_{21}$,[13] resulting in quantum mechanical transition rate $W_{2\rightarrow 1}$ as follows

$$W_{2\rightarrow 1} = \frac{2\pi}{\hbar}|H'_{21}|^2 \rho_f (E_1 = E_2 - \hbar\omega_0), \tag{1}$$

where ρ_f is the density of the final states, and $\hat{H}'_{21}$ can be expressed as a function of the transition matrix element $|M_T|^2 = |\langle u_c|\hat{e}\cdot\mathbf{p}|u_v\rangle|^2$ and the envelope functions overlap $|\Gamma_{e\text{-hh}}|^2 = |\langle F_2|F_1\rangle|^2$. The $|u_c\rangle$ and $|u_v\rangle$ refer to the conduction and valence band Bloch functions, respectively, while the $|F_2\rangle$ and $|F_1\rangle$ are the envelope electron and hole wave functions, respectively. For spontaneous recombination, the transition matrix element term reduces to $|\langle u_c|u_v\rangle|^2$ as the emission is initiated by energy fluctuations in the vacuum state.[14] Therefore, radiative recombination rate and optical gain of III-nitride QWs can be enhanced by engineering the nanostructures with improved overlap $\Gamma_{e\text{-hh}}$.

Previously, improvement in the photoluminescence (PL) and quantum efficiency of InGaN QW via a "two-step metal-organic chemical vapor deposition (MOCVD)"[15] was attributed to the improved material quality resulting from (1) a more homogeneous indium wetting layer due to the trimethylindium (TMIn) prewetting prior to the QW deposition and (2) suppression of the surface-segregated indium from H_2 growth interruption. In contrast to the two-step MOCVD,[15] the radiative efficiency enhancement in our current approach was obtained via optimizing the overlap $\Gamma_{e\text{-hh}}$ for the specific QW active region emitting at a particular wavelength by using staggered InGaN QW structures.

To analyze the InGaN QW structure design, we have developed a numerical framework based on model solid theory utilizing the Kane model for wurtzite band edge energies and the Luttinger-Kohn model for the band structure parameters. The band parameters for the III-nitride alloys were obtained from Refs. 16–22. The GaN electron effective mass constants of $0.18m_o$ and $0.2m_o$ were used for the c axis and the transverse direction, respectively.[17] The InN electron effective mass of $0.11m_o$ was used for both the c axis and the transverse directions.[17] The heavy hole effective masses were calculated following the treatment presented in Ref. 19. The energy gap of the InGaN QW is calculated using a bowing parameter of 1.4 eV (Ref. 16) and an InN energy gap of 0.6405 eV,[21] with $\Delta E_c : \Delta E_v$ of 70:30.[20] The strain effect is taken into account in the form of band edge energy shifts, and the polarization-induced electric field is manifested in the energy band bending. The spontaneous polarization P_{sp} (C/m^2) and piezoelectric polarization P_{pz} (C/m^2) in the InGaN QW were calculated using the following relations:[22]

$$P_{\text{sp}}(x) = -0.042x - 0.034(1-x) + 0.037x(1-x), \tag{2}$$

$$P_{\text{pz}}(x) = 0.148x - 0.0424x(1-x), \tag{3}$$

with x as the In content in the QW. The quantum-confined energy levels of electron and hole were computed using ef-

[a]Electronic mail: raa4@lehigh.edu
[b]Electronic mail: tansu@lehigh.edu

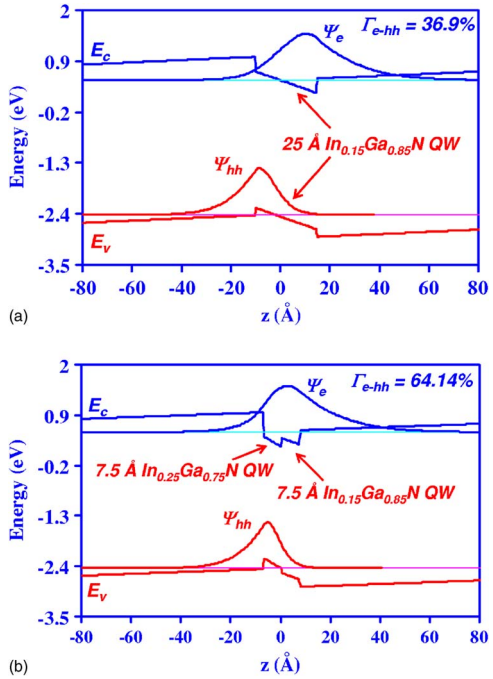

FIG. 1. (Color online) Energy band lineups of (a) 25 Å conventional type-I $In_{0.25}Ga_{075}N$ QW and (b) staggered 7.5 Å $In_{0.25}Ga_{0.75}N$/7.5 Å $In_{0.15}Ga_{0.85}N$ QW.

fective mass approximation with propagation matrix (mesh size=0.5 Å).[23] In our studies, the conventional and staggered InGaN QWs were designed for emission at a particular wavelength regime, with the staggered QWs designed for optimized overlap at that regime. Thus, the In contents and layer thicknesses in the conventional and staggered QWs should not be construed as being related to one another.

Figure 1(a) shows the band lineup of 25 Å $In_{0.15}Ga_{0.85}N$ QW surrounded by GaN barriers with its corresponding electron and hole wave functions for emission at λ_{peak}=427.5 nm regime. The polarization fields in the conventional InGaN QW lead to a low overlap $\Gamma_{e\text{-hh}}$ of only 36.9%. The staggered QW structures (designed for λ_{peak}=421 nm) consist of 7.5 Å $In_{0.25}Ga_{0.75}N$/7.5 Å $In_{0.15}Ga_{0.85}N$ layers surrounded by GaN barriers, as shown in Fig. 2. The use of staggered InGaN QWs leads to the "pulling" of electron wave function from the right to the center of the QW due to the lighter electron effective mass in contrast to that of the hole. The hole wave function is relatively unchanged due to the heavier hole effective mass. As a result, the overlap $\Gamma_{e\text{-hh}}$ for the staggered InGaN QWs is increased to 64.14%. An improvement of the overlap ($\Gamma_{e\text{-hh}}$) by a factor of 1.74 translates to ~3.02 times improvement in radiative recombination rate and optical gain of the active region.

Experiments had been conducted to compare the optical properties of staggered InGaN QWs and conventional InGaN QW, with emission wavelength at 420–430 nm. Both the conventional and staggered InGaN QW samples were grown by MOCVD on 2.5-μm-thick undoped GaN (T_g=1080 °C) grown on *c*-plane sapphire, employing a low temperature 30 nm GaN buffer layer (T_g=535 °C). The conventional QW structure consists of four periods of 25 Å $In_{0.15}Ga_{0.85}N$ QW, while the staggered QW structure is formed by four periods of 7.5 Å $In_{0.25}Ga_{0.75}N$/7.5 Å $In_{0.15}Ga_{0.85}N$ layers. We employed 12 nm GaN barriers in both QW structures. All the active and barrier regions in the structures studied were

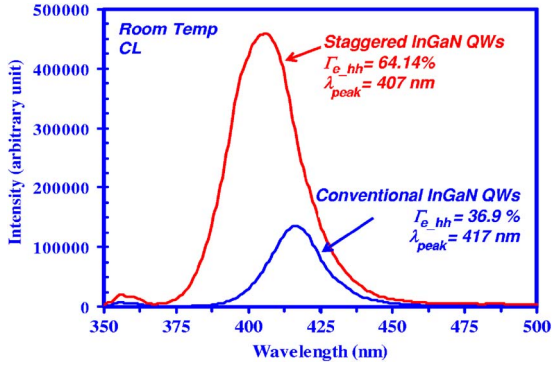

FIG. 2. (Color online) Room temperature cathodoluminescence spectra of staggered 7.5 Å $In_{0.25}Ga_{0.75}N$/7.5 Å $In_{0.15}Ga_{0.85}N$ QW and 25 Å conventional type-I $In_{0.25}Ga_{0.75}N$ QW.

grown at a temperature of 720 °C. The composition and growth rate of the $In_xGa_{1-x}N$ alloy were calibrated individually for a particular composition using high-resolution x-ray diffraction (XRD) measurements. The *staggered* InGaN QW is then realized using growth conditions (gas flows, V/III ratio, growth rate and duration, temperature, and growth pressure) obtained from this calibration. The In content and thicknesses for QW structures are then verified by comparing the peak PL wavelengths with the data from XRD calibration and numerical model.

Room temperature cathodoluminescence (RT-CL) measurements were performed utilizing 10 keV electron beam with 1 μA of current over a raster scan area size of 800 $\times$600 μm^2, with an integration time of 0.1 s. The CL emission wavelengths for staggered QW and conventional QW are measured as 407 and 417 nm, respectively. The CL emissions of both the staggered and conventional QWs were blueshifted by 10–15 nm in comparison to those of the photoluminescence wavelengths, presumably due to larger carrier screening effect in CL measurements. As shown in Fig. 2, the staggered QW structure exhibited an increase of CL peak intensity and integrated luminescence intensity by factors of 3.37 and 4.15 times, respectively, in comparison to those of the conventional QW.

RT-PL measurements were also performed on both samples using 325 nm He–Cd lasers. The PL peak emission wavelengths (λ_{peak}) of the staggered QW and conventional QW were measured as 420 and 430 nm, respectively. The peak PL and integrated PL luminescence intensities for the staggered $In_{0.25}Ga_{0.75}N/In_{0.15}Ga_{0.85}N$ QWs exhibited improvement by factors of 4.74 times and 4.39 times, respectively, in comparison to those of the conventional $In_{0.25}Ga_{0.75}N$ QW. It is also important to point out that integrated luminescence improvement in the staggered InGaN QW is not accompanied by increased linewidth, rather it is attributed to higher peak intensity at the same excitation laser power. This is consistent with the fact that the measurements were conducted at the same temperature, employing identical optical excitation power to facilitate direct spectrum comparison. The PL full width at half maximum (FWHM) for staggered InGaN QWs is measured as 14.8 nm (106.2 meV), which is comparable to that of the conventional InGaN QW (FWHM=17.3 nm or 113.8 meV). The comparable PL FWHMs indicate that the material qualities of both the staggered and conventional InGaN QWs are similar.

To further extend the concept of staggered InGaN QW emitting at longer wavelength, we conducted experiments

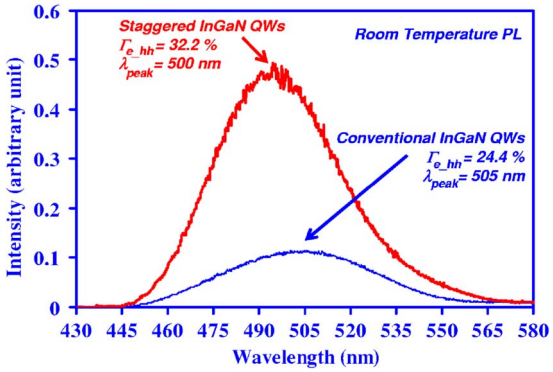

FIG. 3. (Color online) Room temperature photoluminescence spectra of staggered 13 Å $In_{0.28}Ga_{0.72}N$/13 Å $In_{0.21}Ga_{0.79}N$ QW and 27 Å conventional $In_{0.26}Ga_{0.74}N$ QW.

utilizing 27 Å conventional $In_{0.26}Ga_{0.74}N$ QW ($\Gamma_{e\text{-hh}}$ =24.4%) and staggered 13 Å $In_{0.28}Ga_{0.72}N$/13 Å $In_{0.21}Ga_{0.79}N$ QW ($\Gamma_{e\text{-hh}}$=32.2%), emitting at λ_{peak} =500–515 nm. As shown in Fig. 3, the staggered $In_{0.28}Ga_{0.72}N/In_{0.21}Ga_{0.79}N$ QW exhibited improvements in the peak PL and the total integrated PL luminescence intensity by 4.48 and 3.54 times, respectively. The staggered QW structure exhibited an increase of CL peak intensity and integrated luminescence intensity by factors of 2.1 and 2.43 times, respectively, in comparison to those of the conventional QW. The observed PL and CL improvements were higher than those predicted from the increase in overlap $\Gamma_{e\text{-hh}}$ alone.

To assess the staggered QWs for device applications, we realized two LED structures (λ_{peak}=455–465 nm) utilizing (1) four periods of staggered QWs of 12 Å $In_{0.25}Ga_{0.75}N$/12 Å $In_{0.15}Ga_{0.85}N$ layers ($\Gamma_{e\text{-hh}}$=43.1%) and (2) four periods of 27 Å conventional $In_{0.21}Ga_{0.79}N$ QW ($\Gamma_{e\text{-hh}}$=27.4%) as the active regions of each LEDs. Both structures were grown on 2.5 μm n-GaN template ($n=3\times10^{18}$ cm^{-3}) on c-plane sapphire substrates. The acceptor level for the p-GaN layer is 3×10^{17} cm^{-3}. Continuous wave power measurements were performed at room temperature. Figure 4 shows that the output power is linear as function of driving current up to 100 mA for both LEDs with an area of 1 mm^2. Staggered QW LEDs exhibited an improvement in output power by 11.2 times at a current level of 100 mA. The measured significant enhancement is larger than that predicted theoretically, and several possible factors may contribute to this improvement, such as (1) more pronounced carrier screening reduces energy band bending and further increases overlap $\Gamma_{e\text{-hh}}$, (2) improved material quality, and (3) better carrier confinement in the staggered InGaN QWs. Further studies and optimizations are still required to elucidate more insights into the physics of polarization engineering of Nitride-based active regions, in particular, recombination analysis and structural analysis of the staggered InGaN QW are needed to clarify the factors leading to this improvement.

In summary, polarization band engineering using staggered InGaN QWs with improved overlap ($\Gamma_{e\text{-hh}}$) leads to significant enhancement of radiative recombination rate. Improvements in PL peak luminescence intensity and integrated luminescence by factors of 4.74 and 4.39 times (and 4.48 and 3.54 times), respectively, had been experimentally demonstrated for staggered InGaN QWs active regions emitting at

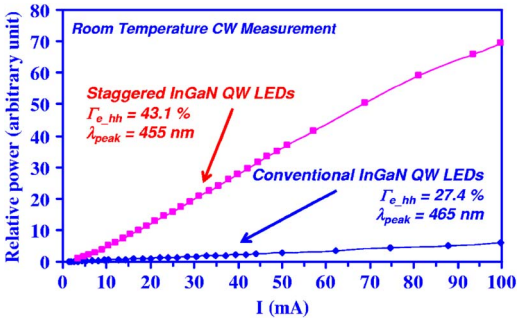

FIG. 4. (Color online) Relative light output power vs injected current for staggered 12 Å $In_{0.25}Ga_{0.75}N$/12 Å $In_{0.15}Ga_{0.85}N$ QW LED and 27 Å conventional $In_{0.21}Ga_{0.79}N$ QW LED.

λ_{peak}=420–430 nm (and λ_{peak}=500–505 nm), which are in good agreement with the theory. Preliminary LED had also been fabricated utilizing staggered InGaN QW emitting in λ_{peak}=455–465 nm, resulting in almost an order of magnitude improvement in the output power of the devices. The use of polarization control for enhancing the $\Gamma_{e\text{-hh}}$ of the InGaN-based active regions can be applicable for high-efficiency LEDs and low-threshold Nitride-based lasers.

The authors would like to acknowledge funding support from US Department of Defense, ARL and National Science Foundation (NSF) under Award No. 0701421.

[1] S. Nakamura, M. Senoh, N. Iwasa, S. Nagahama, T. Yamada, and T. Mukai, Jpn. J. Appl. Phys., Part 2 **34**, L1332 (1995).
[2] S. Nakamura, M. Senoh, S. Nagahama, N. Iwasa, T. Yamada, T. Matshushita, H. Kiyoku, and Y. Sugimoto, Jpn. J. Appl. Phys., Part 2 **35**, L74 (1996).
[3] S. Chhajed, Y. Xi, Y.-L. Li, Th. Gessmannand, and E. F. Schubert, J. Appl. Phys. **97**, 054506 (2005).
[4] W. Zhao, Y. Li, T. Detchprohm, and C. Wetzel, Phys. Status Solidi C **4**, 9 (2007).
[5] R. H. Horng, C. C. Yang, J. Y. Wu, S. H. Huang, C. E. Lee, and D. S. Wuu, Appl. Phys. Lett. **86**, 221101 (2005).
[6] J. S. Cabalu, A. D. Williams, T. C. P. Chen, R. France, and T. D. Moustakas, Mater. Res. Soc. Symp. Proc. **892**, 0892 (2006).
[7] J. Zhang, J. Yang, G. Simin, M. Shatalov, M. Asif Khan, M. S. Shur, and R. Gaska, Appl. Phys. Lett. **77**, 2668 (2000).
[8] T. Deguchi, K. Sekiguchi, A. Nakamura, T. Sota, R. Matsuo, S. Chichibu, and S. Nakamura, Jpn. J. Appl. Phys., Part 2 **38**, L914 (1999).
[9] F. Bernardini, V. Fiorentini, and D. Vanderbilt, Phys. Rev. B **56**, R10024 (1997).
[10] F. Bernardini and V. Fiorentini, Phys. Rev. B **57**, R9427 (1998).
[11] S. Nagahama, Y. Sugimoto, T. Kozaki, and T. Mukai, Proc. SPIE **5738**, 57, (2005).
[12] C. Wetzel, S. Kamiyama, H. Amano, and I. Akasaki, Jpn. J. Appl. Phys., Part 1 **41**, 11 (2002).
[13] L. A. Coldren and S. W. Corzine, *Diode Lasers and Photonic Integrated Circuits* (Wiley, New York, 1995), p. 513.
[14] J. Singh, *Electronic and Optoelectronic Properties of Semiconductor Structures* (Cambridge University Press, Cambridge, 2003), p. 355.
[15] T. Bottcher, F. Bertram, P. Bergman, A. Ueta, J. Christen, and D. Hommel, Mater. Res. Soc. Symp. Proc. **798**, Y5.59.1 (2004).
[16] I. Vurgaftman and J. R. Meyer, J. Appl. Phys. **94**, 3675 (2003).
[17] J. Piprek, *Semiconductor Optoelectronic Devices: Introduction to Physics and Simulation* (Academic, London, 2003), p. 34.
[18] S. L. Chuang, IEEE J. Quantum Electron. **32**, 1791 (1996).
[19] S. L. Chuang and C. S. Chang, Phys. Rev. B **54**, 2491 (1996).
[20] Y. C. Yeo, T. C. Chong, M. F. Li, and W. J. Fan, J. Appl. Phys. **84**, 1813 (1998).
[21] J. Wu, W. Walukiewicz, W. Shan, K. M. Yu, J. W. Ager III, S. X. Li, E. E. Haller, H. Lu, and W. J. Schaff, J. Appl. Phys. **94**, 4457 (2003).
[22] O. Ambacher, J. Majewski, C. Miskys, A. Link, M. Hermann, M. Eickhoff, M. Stutzmann, F. Bernardini, V. Fiorentini, V. Tilak, W. J. Schaff, and L. F. Eastman, J. Phys.: Condens. Matter **14**, 3399 (2002).
[23] S. L. Chuang, *Physics of Optoelectronic Devices* (Wiley, New York, 1995), p. 157.